RSC Advances

PAPER

View Article Online
View Journal | View Issue

Published on 22 January 2015. Downloaded by UNIVERSIDADE FEDERAL SAO CARLOS on 4/29/2019 6:13:09 PM.

Cite this: *RSC Adv.*, 2015, **5**, 12000

Vanadium pentoxide 1-D nanostructures applied to dye removal from aqueous systems by coupling adsorption and visible-light photodegradation†

Waldir Avansi Jr,*[a] Vagner R. de Mendonça,[ab] Osmando F. Lopes[bc] and Caue Ribeiro[c]

This paper evaluates the photocatalytic and dye adsorption properties of highly crystalline orthorhombic vanadium pentoxide (V_2O_5) one-dimensional (1D) nanostructures, such as nanowires and nanorods, synthesized by a hydrothermal method. The as-synthesized samples were characterized by X-ray diffraction (XRD), UV-vis diffuse reflectance spectroscopy (DRS), scanning and transmission electron microscopy (SEM and TEM), thermogravimetry (TGA), zeta potential, Fourier transform infrared spectrometry (FTIR), N_2 adsorption isotherms and high-resolution ^{13}C nuclear magnetic resonance (NMR). The dye adsorption capability and photocatalytic properties under visible light were mainly studied by the removal of the methylene blue dye (MB). Despite their low specific surface area (approximately 35 m^2 g^{-1}), the nanostructures showed high MB adsorption capabilities of greater than 400 mg g^{-1}. Additionally, due to the band-gap values (approximately 2.6 eV), the nanostructures could be successfully applied to photodegradation under visible light, showing higher photoactivity than commercial V_2O_5. The MB adsorption mechanism onto V_2O_5 1D-nanostructures surface can be explained *via* NMe_2^+ interaction with the negatively charged surface of the studied samples. The observed combination of adsorbent and photocatalytic properties makes the V_2O_5 1D-nanostructures a promising material for organic pollutant decontamination, which appears more efficient for cationic species.

Received 20th October 2014
Accepted 9th January 2015

DOI: 10.1039/c4ra12788a

www.rsc.org/advances

1. Introduction

Water contamination by pollutants, such as dyes or pesticides, has caused several environmental problems, attracting the attention of many researchers in the development of efficient methods for removing these pollutants.[1–4] Several techniques have been used for water treatment, such as coagulation, chemical oxidation, adsorption and photodegradation.[1–5] Among those methods, the process of adsorption and photodegradation by applying a heterogeneous photocatalyst appear to be an interesting and efficient method because both processes can be combined into one step.[1,6] Indeed, adsorption is one of the most effective dye-removal methods in water systems; this process converts pollutants from aqueous suspension to solid phase rather than causing their degradation.[7] However, solid adsorbents present limited adsorption capacity because saturated adsorbents require further regeneration or replacement to be applied in a continuous process.[6] Conversely, heterogeneous photocatalysis is based on the formation of radicals with high oxidative potential, which can lead to overall degradation of a wide variety of organic pollutants.[8,9] In this way, combined adsorption–photocatalysis, leading to the *in situ* regeneration of adsorption sites, can improve the global process leading to photocatalytic materials with higher performance.[8,10]

Previous studies have focused on composites containing adsorbent and photocatalytic materials.[10–13] Composites of TiO_2 with activated carbon[10] and TiO_2 with SiO_2 [13] have presented higher pollutant removal efficiencies compared with the isolated phases. On the other hand, additional studies have shown the application of one phase, which acts as an adsorbent and photocatalyst concomitantly.[14,15] For example, Kim *et al.*[15] showed the high efficiency of BiOCl in Rhodamine B, methyl orange and methylene blue dye removal due to the special characteristics of the material, which simultaneously exhibited photocatalytic and adsorbent properties.

Vanadium pentoxide (V_2O_5) is a semiconductor with a band-gap ranging from 2.3 to 2.8 eV with special surface properties.[16–20] V_2O_5 possesses high surface acidity, a high specific surface area, and have great potential for use in various applications,[16–20] such as photocatalysis under visible light[21,22] and adsorption.[23] In this sense, V_2O_5 may be suitable for dye removal

[a]*Departamento de Física, Universidade Federal de São Carlos, São Carlos-SP, Brasil. E-mail: wavansi@pq.cnpq.br*

[b]*Departamento de Química, Universidade Federal de São Carlos, São Carlos-SP, Brasil*

[c]*Laboratório Nacional de Nanotecnologia para Agricultura (LNNA) – Embrapa Instrumentação, São Carlos-SP, Brasil*

† Electronic supplementary information (ESI) available. See DOI: 10.1039/c4ra12788a

This journal is © The Royal Society of Chemistry 2015

Published on 22 January 2015. Downloaded by UNIVERSIDADE FEDERAL SAO CARLOS on 4/29/2019 6:13:09 PM.

applications by coupling its adsorption and photocatalytic properties, and fine-tuning the electronics and surface properties of the crystalline structures during the synthesis process.

The synthesis method plays an important role in the development of high-performance photocatalytic/adsorbents materials due to the dependence of certain characteristics, such as crystalline phase, electronic structure and surface features, on the synthesis conditions.[24–27] Though several strategies have been developed for the hydrothermal synthesis of V_2O_5 nanostructures,[28,29] our group reported an interesting strategy for the synthesis of $V_2O_5 \cdot nH_2O$ nanostructures with morphology and crystal structure controlled using a hydrogen peroxide method.[30] This process possesses several advantages in the synthesis of nanostructures, namely, the elimination of foreign ions or organic ligands and control of morphology and crystal structure through synthesis variables.[24,30] Indeed, our research group has published various studies employing the hydrogen peroxide method combined with hydrothermal treatment to prepare different nanostructures.[30–35]

The main goal of this research is to outline, simple method for contaminant removal based on the orthorhombic $V_2O_5 \cdot nH_2O$ (1D) nanostructures produced by peroxide vanadium complex decomposition under hydrothermal treatment. Methylene blue (MB) dye in aqueous system was used as a model contaminant, to study the coupled adsorptive–photocatalytic properties. Despite previous papers separately describing V_2O_5 adsorptive[23] and photocatalytic properties,[21,22] an evaluation regarding the coupled properties (adsorption–photocatalytic under visible-light irradiation) of V_2O_5 (1D) nanostructures is still open.

2. Materials and methods

2.1. Synthesis

The synthesis of $V_2O_5 \cdot nH_2O$ nanostructures is described in greater detail in ref. 30, it is based on the dissolution of V_2O_5 micrometric powder (Alfa Aesar, 99.995% purity), denoted here as a precursor, in distilled water with the addition of the appropriate amount of hydrogen peroxide (H_2O_2 30%) and subjected to the hydrothermal treatment. The deeper morphological and structural characterizations can be checked in great details elsewhere.[30,36,37] As reported in our previous works, in these synthesis conditions, the presence of water molecules do not lead to any significant structural changes being mainly related to adsorbed water.[30,36] In this sense, we denoted the samples as V_2O_5 (1D) nanostructures. To obtain V_2O_5 (1D) nanostructures with different morphologies, the hydrothermal treatment was conducted at two different temperatures for a 24 hours period. The samples obtained at 180 °C in hydrothermal treatment were denoted as SAM01, whereas the SAM02 sample were developed at 200 °C.

2.2. Characterizations

The material's crystalline structure was determined by X-ray diffraction (XRD) through a Shimadzu XRD 6000 diffractometer with Cu Kα radiation in a continuous scan mode; the scan speed was 2° min^{-1} with a step of 0.02°. The size and morphology of the nanostructures was determined by scanning electron microscopy (SEM) using a JEOL JSM-6510 and by transmission electron microscopy (TEM), using a JEOL JEM 2100 operated at 200 keV.

The specific surface area (SA) was measured by the nitrogen physical adsorption at 77 K using a Micromeritics ASAP 2020 particle size analyzer. The isotherm data were treated using the standard BET (Brunauer–Emmett–Teller) method.

UV-visible diffuse reflectance spectra (DRS) were acquired employing a Cary 5G spectrophotometer in the 200–800 nm range and were recalculated using the Tauc method and normalized.[38] The band-gap of each sample was calculated by plotting the absorption coefficient, $(\alpha h\nu)^2$, against the photon energy, $h\nu$, according to the following equation: $\alpha h\nu = A(h\nu - E_g)^{1/2}$, where E_g describes the band gap for direct transitions and A is a constant.[38]

The zeta potential of the dilute suspensions was measured in a Zeta Potential Meter (Malvern – ZetaSizer model nano-ZS) in a pH range of 8 to 3: the pH value was adjusted by adding HCl or KOH.

2.3. Dye removal by visible-light photodegradation and adsorption

V_2O_5 photocatalytic and adsorption properties were evaluated by quantifying the removal of MB. For the photocatalytic experiments, the samples were immersed in 20 mL of an aqueous solution of MB (20 mg L^{-1}). The beakers were placed in a photo-reactor at controlled temperature (20 °C) with six lamps (Philips visible light lamps, 15 W). The removal of MB was monitored using a spectrophotometer (Shimadzu-UV-1601 PC) to measure the intensity of the characteristic UV-vis absorption peak (at 663 nm) following different durations of light exposure. To check the influence of adsorption during the irradiation, the same experiments were performed without irradiation, and the decay in MB concentration was determined in the same way.

The adsorption capability of the as-synthesized sample was determined by the adsorption isotherms obtained in dark condition under 25 °C using a 150 mg L^{-1} powder sample concentration suspended in the MB solution ranging from 25 to 500 mg L^{-1}. The suspensions magnetically stirred during a 24 h period to reach the adsorption–desorption equilibrium. After this period, the adsorption performance was measured by the decrease in MB concentration. In order to check the adsorption mechanism and capability, Rhodamine B (RhB, 50 mg L^{-1}, neutral charge) and methyl orange (MO, 50 mg L^{-1}, anionic dye), which possesses different structure and electronic characteristics, were studied under the same conditions applied to MB adsorption studies.

To evaluate the MB dye desorption onto the substrate, the kinetics of desorption studies was performed. Firstly, the SAM02 sample with MB adsorbed (100 mg L^{-1}) was stirred in ethanol, at regular time intervals, then the samples were collected and MB concentration was measured in a UV-vis spectrophotometer. The ethanol was chosen due to its better

Published on 22 January 2015. Downloaded by UNIVERSIDADE FEDERAL SAO CARLOS on 4/29/2019 6:13:09 PM.

interaction with MB dye when compared to water and other solvents.[39]

To check the presence of MB molecules adsorbed onto the as-synthesized nanostructures and their stability, the samples were separated through centrifugation, and then characterized by thermogravimetric analysis (TGA), Fourier transform infrared spectroscopy (FTIR), Raman spectroscopy, XRD patterns and high-resolution ^{13}C nuclear magnetic resonance (NMR). For this analysis, we used the powders from MB solution with initial concentration of 50 mg L^{-1}. FTIR analysis data were collected in a Perkin Elmer Spectrum 1000. The samples were firstly kept at a constant temperature of 100 °C for 12 h and were then placed in a desiccator to ensure the same atmospheric conditions for all the samples prior to FTIR analysis. The TGA was performed using a TA Q500 thermogravimetric analyzer under the following conditions: weight (10.0 ± 0.5) mg; synthetic air flow 60 mL min^{-1}; heating rate of 10 °C min^{-1}; and temperature range 30–700 °C. Raman spectrum was acquired using Raman spectrometer (Horiba Jobin-Yvon) coupled to a microscope (Olympus TM BX41). An Ar^+ ion laser using the 514.5 nm laser line provided the spectral excitation. A low power laser was used to prevent the laser beam from changing the characteristics of the samples. The XRD measurement was performed under the same conditions described before.

Spectra of solid-state ^{13}C NMR with variable amplitude, cross-polarization and magic angle spinning (VACP/MAS) were obtained in a spectrometer Bruker (Avance III HD) operating at a frequency of 400 MHz for 1H and 100.59 MHz for ^{13}C, under the following experimental conditions: 10 kHz spinning speed, with the contact time of 45 ms and relaxation time of 5 s. About 50 mg of SAM02 + MB and MB pure were packed in a 5 mm cylindrical zirconium rotor with Kel-F end-caps. The chemical shift values were calibrated using tetramethylsilane as a reference. In order to better the signal-to-noise ratio, 16 384 scans were performed on each sample. To identify the chemical shifts related to each carbon in a MB dye molecular structure, a simulation was performed using the NMR-Predictor program (available at http://www.nmrdb.org/).

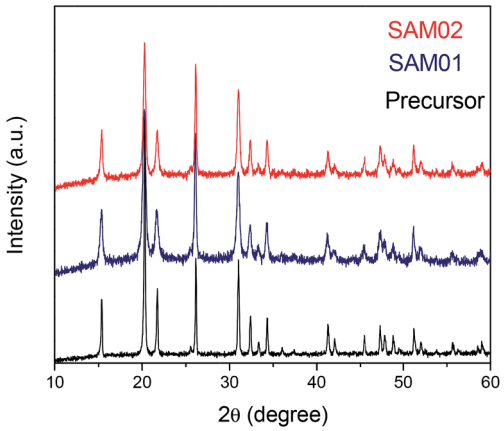

Fig. 1 XRD patterns of the oxide precursor and the as-synthesized samples: SAM01 (180 °C/24 h) and SAM02 (200 °C/24 h). All of the peaks are related V_2O_5 orthorhombic phase (PDF#85-0601).

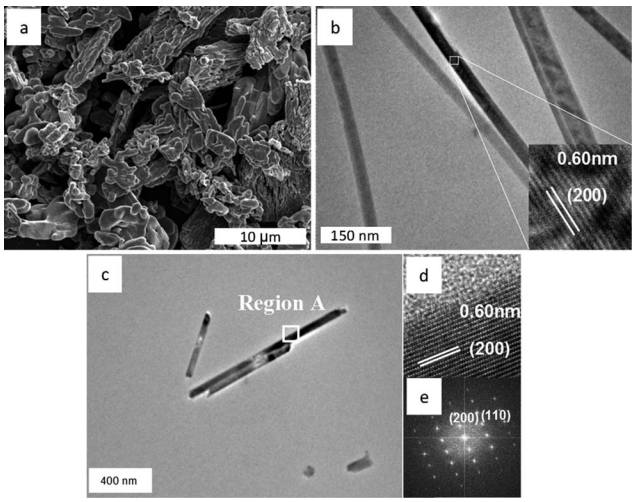

Fig. 2 (a) SEM image of the precursor sample; and TEM images of (b) the samples SAM01 and (c) SAM02; (d) HRTEM images of region A; (e) Fourier transform of region A.

3. Results and discussions

Fig. 1 presents the XRD patterns of the as-synthesized samples and the material employed as the precursor. As expected, the patterns are indexed as the V_2O_5 orthorhombic phase (PDF#85-0601).

From Fig. 1, it is clear that the samples (SAM01 and SAM02) and the precursor presented the same crystalline phase; therefore, the main differences between the samples should be related to their morphology and/or surface features, because SAM01 and SAM02 may contain a small amount of adsorbed water due to the synthesis conditions.[30]

Electron microscopy was employed to analyze the precursor and as-synthesized samples morphologies, and the results are shown in Fig. 2. SEM image in Fig. 2a shows the precursor (orthorhombic phase V_2O_5) with a granular morphology with micrometric sizes between 2–5 μm. TEM images in Fig. 2b and c show that SAM01 and SAM02 present nanowire and nanorod morphologies, respectively, as reported before in our previous work.[30] Moreover, HRTEM images of SAM01 (insets on Fig. 2b) and SAM02 (Fig. 2d) show the single crystalline nature of the synthesized materials, with an interplanar distance of approximately 0.60 nm, which corresponds to the (200) crystallographic plane in V_2O_5 orthorhombic phase (PDF#85-0601). These features and the Fast Fourier Transform (FFT) of Fig. 2d confirms the single crystalline nature of the as-synthesized samples and the fact that the growth occurs preferentially along the [010] direction (nanoparticle length), Fig. 2e.[30,36] The diameters observed for SAM01 and SAM02 were approximately 25 and 40 nm, respectively, where the increase in diameter size in different synthesis conditions could be attributed primarily to the laterally oriented attachment growth mechanism that was previously examined by our group.[36] The specific surface area (SA) of the samples was determined as 35 m^2 g^{-1} for SAM01 and 28 m^2 g^{-1} for SAM02, which is in accordance with the

 This journal is © The Royal Society of Chemistry 2015

Published on 22 January 2015. Downloaded by UNIVERSIDADE FEDERAL SAO CARLOS on 4/29/2019 6:13:09 PM.

morphological features observed for these samples, since SAM02 showed a greater diameter compared to SAM01.

Fig. 3 presents the UV-DRS spectra for both as-obtained samples (SAM01 and SAM02) and for the samples employed as precursor. The UV-DRS spectra are recalculated by the Tauc method to measure the band-gap values (inset of Fig. 3).[38] Despite the differences in morphology, the band-gap of the as-synthesized samples showed only a slight difference, with a band-gap in the visible region of the electromagnetic spectrum, 486 nm (2.55 eV) and 476 nm (2.60 eV) for SAM01 and SAM02, respectively. The sample denoted as precursor (commercial V_2O_5), also presented a band-gap in the visible region around 560 nm (2.2 eV). The UV-DRS results are in good agreement with previous report in literature.[16–20]

The development of high efficiency visible light active photocatalysts remains a challenge for many researchers.[40–43] The most studied semiconductors for photocatalytic application (TiO_2,[24] ZnO)[27] can only be activated under UV radiation, which represents only 4–5% of the sunlight.[42] Therefore, the bang-gap values are an important feature of the as-synthesized samples, showing the possibility for photocatalysis activated by wavelengths higher than 470 nm, *i.e.*, in visible light region.

The coupled photocatalytic and adsorbent properties of the precursor and the as-synthesized samples were firstly evaluated by the removal of MB. Fig. 4 shows the results of adsorption (in dark conditions) and photodegradation coupled to adsorption (irradiated conditions) over time. The MB self-photolysis was also evaluated for solutions without any catalyst, designated "blank". It is worth noting that the samples SAM01 and SAM02 exhibited an MB adsorption of approximately 17% for both samples, this is an improvement over the precursor sample, which did not show significant MB adsorption.

As observed in the graph (Fig. 4), the precursor sample showed the worst photoactivity and adsorption properties; even under irradiation for 210 minutes, the MB concentration decreased by less than 10%. In the presence of as-synthesized samples under irradiation, MB concentration decreased of by

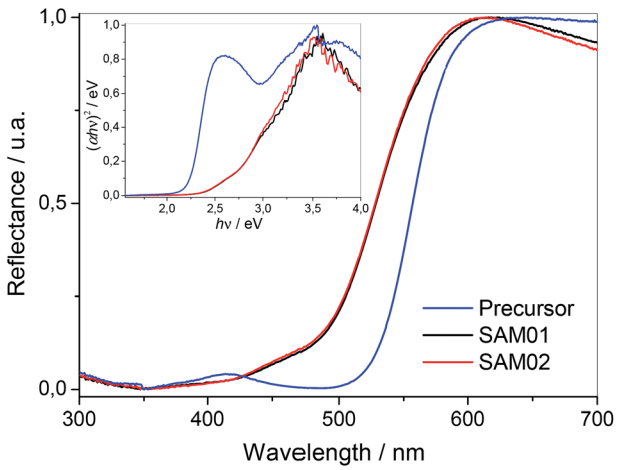

Fig. 3 (a) UV-visible diffuse reflectance spectra (DRS) of synthesized samples. (b) A plot of $(\alpha h\nu)^2$ *vs.* photon energy ($h\nu$) obtained by the Tauc equation[38] from DRS spectra.

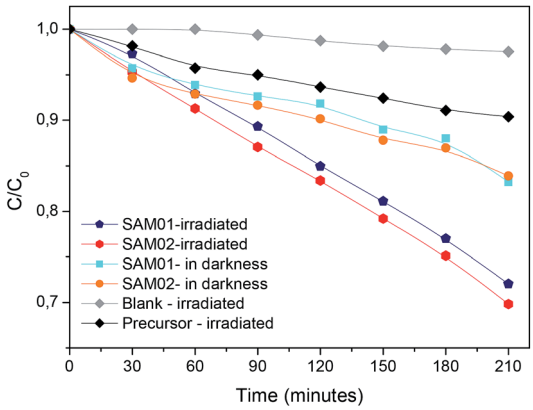

Fig. 4 Photodegradation coupled to adsorption under visible light and adsorption (in darkness) of MB (20 mg L^{-1}) over the as-synthesized samples.

28% and 31% for SAM01 and SAM02, respectively. Therefore, these experiments showed the synergistic effect of adsorption and photodegradation for MB removal from water.

It is interesting to note the fact that the small observed changes in morphological and textural properties for the SAM01 and SAM02 samples did not lead to a significant difference in MB photodegradation. The similarities in the photocatalytic performance could be related to the different properties that influence the overall process, since heterogeneous photocatalysis is dominated by two main variables: the specific surface area and the charge carrier recombination rate.[24,35]

Because both samples showed high adsorption capacity in the coupled experiment for MB, we studied the MB adsorption isotherm for SAM02 sample (Fig. 5) to understand the interaction between adsorbate and adsorbent; we chose only one sample due to the similarity between the performance of SAM01 and SAM02 in the previous tests. The as-synthesized V_2O_5 nanostructures had a high MB adsorption capacity of 437 mg g^{-1} (Fig. 6a), when compared with other materials; $W_{18}O_{49}$ [44] and composite TiO_2/polypyrrole[45] are measured having adsorption capacities of 201 mg g^{-1} and 273 mg g^{-1}, respectively. The data were fitted by the Langmuir isotherms given in eqn (1).

$$\frac{C_{eq}}{Q_{eq}} = \frac{1}{Q_{max}K_L} + \frac{C_{eq}}{Q_{max}} \quad (1)$$

C_{eq} (mg L^{-1}) is the MB equilibrium concentration; Q_{max} (mg g^{-1}) is the maximum adsorption capacity; K_L (L mg^{-1}) is a constant that related to the heat of adsorption.

Fig. 5b illustrates the Langmuir models for SAM02 sample; a high degree of linearity was observed, with a correlation coefficient (R^2) of 0.999. According to the Langmuir model, the maximum adsorption of MB on SAM02 was 434 mg g^{-1}, which is not far from the experimental value (437 mg g^{-1}). It is important to highlight the low repeatability of these experiments, possibly due to the high adsorption capability of the samples (always higher than 400 mg g^{-1}). To confirm the

Published on 22 January 2015. Downloaded by UNIVERSIDADE FEDERAL SAO CARLOS on 4/29/2019 6:13:09 PM.

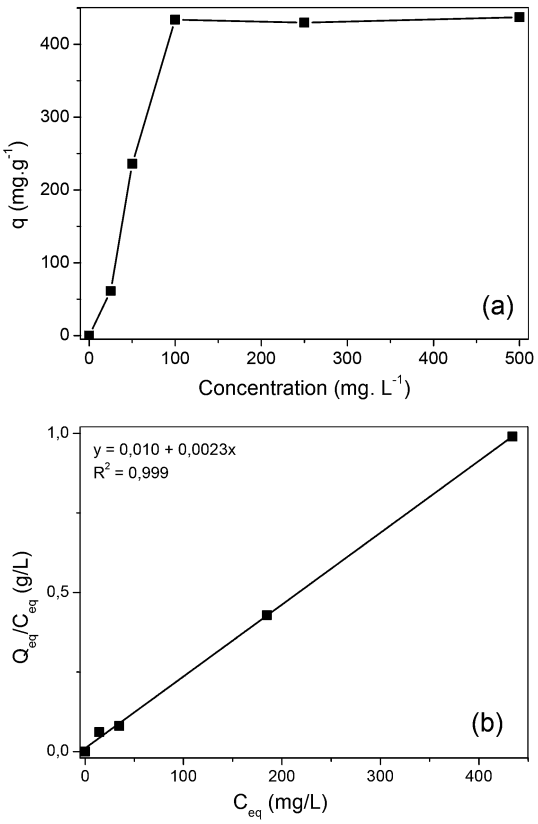

Fig. 5 (a) Adsorption isotherms of methylene blue (MB) without visible light illumination for SAM02 sample; (b) the linear form for Langmuir isotherm model.

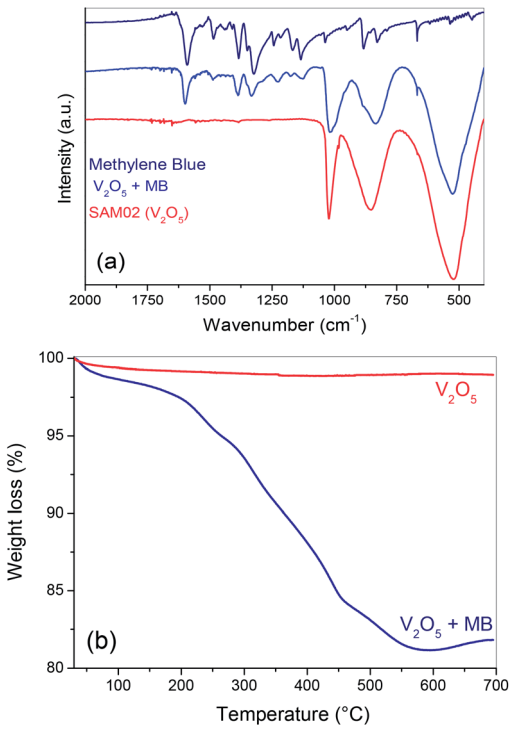

Fig. 6 Analysis of the adsorption product. (a) Infrared spectroscopy of SAM02, V_2O_5 + MB and MB; (b) TGA analysis for SAM02 (V_2O_5) and V_2O_5 + MB.

presence of adsorbed MB molecules, we performed FTIR and TGA analysis of SAM02 after adsorption, Fig. 6.

A question that arises from the adsorption experiments is about the nature of the process: is the decrease in MB caused only by adsorption, or does the dye degrade after interacting with the sample surface? To evaluate the adsorption qualitatively, we obtained the FTIR spectra for SAM02, MB, and the sample containing adsorbed MB (labeled as V_2O_5 + MB); the results are shown in Fig. 6a. In the spectra of V_2O_5 + MB, main peaks related to stretching mode of MB are present. Because those peaks were neither shifted nor omitted after the adsorption process, we can propose that the chemical structure of MB remains intact after adsorption. In other words, the color removal may be related solely to the adsorption and not to the degradation of the chromophore group.

Additionally, we performed TGA analysis after the adsorption process to determine the amount of dye adsorbed on the solid surface, Fig. 6b. The SAM02 sample showed a slight loss, approximately 2 wt%, even at a temperature of 700 °C, as expected, since in employed synthetic conditions only a small amount of adsorbed water was presented.[30] Conversely, the sample after the adsorption (V_2O_5 + MB) showed a loss of approximately 19 wt%. By withdrawing the water adsorbed, this would results in 17 wt% assigned to MB dye. The MB adsorption for V_2O_5 used in TGA experiments was determined to be 230 mg g^{-1} (the MB initial concentration of 50 mg L^{-1}) that represents 19 wt% of MB, which was close to what was expected.

To verify the facility of the MB dye desorption onto the SAM02 sample and how easily it is recycled, the desorption kinetics in ethanol was studied. TGA analysis was used to quantify the MB present in SAM02 sample before the desorption experiment (see Fig. S1a and b†). As a matter of fact, after 120 min of test, around 99% of MB dye was desorbed, which clearly evidenced that SAM02 adsorbent can be easily recycled in those conditions.[39] We also performed XRD, Raman spectroscopy with the powder after the adsorption experiments in order to evaluate the photocatalyst stability (Fig. S2†). Fig. S2a and b† confirm that no structural difference between the pristine SAM02 and SAM02 with MB adsorbed could be observed. This indicates that the dye is not intercalated into the crystal structure, but the two may be chemically linked without changes in crystalline structure.

To understand the adsorption mechanism of the samples, Zeta potential measurements were performed for both synthesized samples revealing that in pH range from 3 to 8 all of the measured values were below −10 mV. This result is indicative of surface acidity in the as-synthesized samples. In fact, at a neutral pH for the MB solution, Zeta potential values were observed at approximately 30 mV. Because MB is a cationic dye with a very high pK_a value (>12), which does not promote the hydrolysis reaction, MB is highly ionized at the pH value of the MB solution.[46,47] Therefore, the MB cations showed strong electrostatic interaction with the negatively charged sample

 This journal is © The Royal Society of Chemistry 2015

Published on 22 January 2015. Downloaded by UNIVERSIDADE FEDERAL SAO CARLOS on 4/29/2019 6:13:09 PM.

surface, explaining the high adsorption values for both samples.

The positive charge in MB dye molecule is delocalized by molecule, *i.e.* resonant, however, this is better stabilized by S and N atoms in N–Me_2 groups (see molecular structure of MB, Fig. 7a).[48] Then, in order to answer which atom (S or N) is responsible for interaction/binding of MB dye at adsorbent surface, the solid state ^{13}C NMR spectra were acquired for the MB pure and SAM02 after adsorption experiments onto SAM02 sample. MB molecule showed 7 carbons with different chemistry environment in ^{13}C NMR spectra (see identification at Fig. 7a), however, the carbons identified how 2 and 3, 5 and 6, respectively, showed a slight shift between them. By comparison of ^{13}C NMR spectra of the SAM02 sample with MB adsorbed and MB pure, main shifts at peaks related to carbon 1 and 7 were observed after their adsorption at SAM02 surface, of 44.4–42.3 ppm and 155–153 ppm, respectively. These shifts can be better visualized in Fig. 7b and c. Carbons 1 and 7 are exactly binding to N atom of NMe_2 group, thus the mechanism of adsorption occurs *via* interaction of NMe_2^+ with negatively charged surface of the SAM02 sample. These results are in agreement with the ones reported by Zhang *et al.*[49] who noticed, through XPS studies, this same behavior to adsorption of MB dye onto carbon nanotubes functionalized with SO_3^- group.

As a matter of fact, we performed some analysis on the adsorption capability in the presence of different dyes, such as RhB and MO, which possesses different structures and electronic characteristic (see Fig. S3a and b†). The adsorption capacity observed for both MO and RhB were 42.3 and 65.5 mg g^{-1} after 3 hours, respectively. The adsorption kinetics presents poor adsorption efficiency compared to MB adsorption capacity of 437 mg g^{-1} (Fig. 6a). In good agreement with the proposed adsorption mechanism, which occurs *via* electrostatic interaction of the negative surface of V_2O_5 with N–Me_2^+ groups of MB, it can be seen that the efficiency of adsorption followed the order of the electronic characteristic of the pollutants: cationic dye (MB) > zwiterrion (neutral-RhB) > anionic dye (MO). Thus, despite the fact that V_2O_5 has potential for adsorption to organic pollutants with different electronic characteristics, it is clear that the adsorption process is more efficient for cationic species.

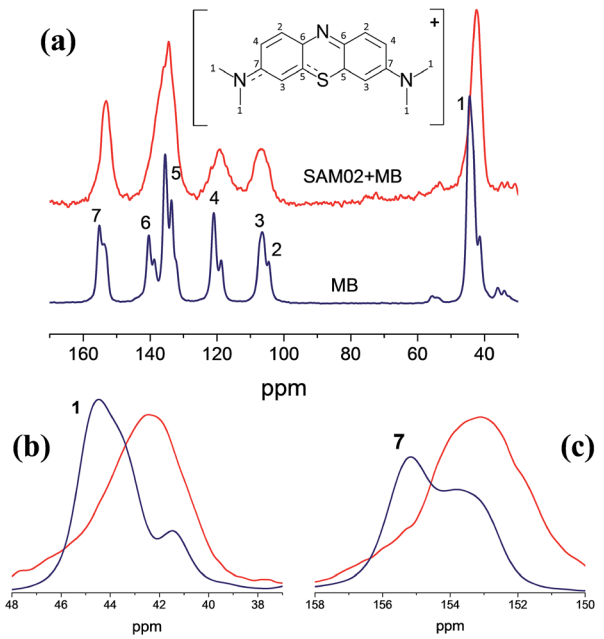

Fig. 7 (a) Solid state ^{13}C VAS/CP NMR spectra of the MB pure and MB adsorbed onto SAM02 sample (SAM02 + MB). (b and c) Spectra with zoom in region assignment to carbon 1 and 7.

4. Conclusions

In summary, orthorhombic vanadium pentoxide (V_2O_5) 1D-nanostructures obtained by the hydrothermal decomposition of vanadium peroxo complex can effectively remove dye from water through a coupled adsorption–photocatalytic process under visible light. Despite its low specific surface area (approximately 35 m^2 g^{-1}), the nanostructures exhibited a high MB adsorption capability, greater than 400 mg g^{-1}. Additionally, the 1D nanostructures could be successfully applied to photodegradation under visible light. The adsorption mechanism occurs mainly *via* interaction of NMe_2^+ with negatively charged surface of as-obtained nanostructures, making the V_2O_5 1D-nanostructures a potentially useful material for the removal of organic pollutants from water, specially for cationic species.

Acknowledgements

The authors gratefully acknowledge the financial support of the Brazilian research funding agencies FAPESP (2013/17639-4) and CNPq. The electron microscopy work has been performed on the Jeol JEM-2100 HT microscope at LME/LNNano/CNPEM, Campinas. We kindly acknowledge MSc. Viviane F. Soares and Dr Luiz A. Colnago by their valuable help in the ^{13}C NMR experiments.

References

1 W. Dong, C. W. Lee, X. Lu, Y. Sun, W. Hua, G. Zhuang, S. Zhang, J. Chen, H. Hou and D. Zhao, *Appl. Catal., B*, 2010, **95**, 197–207.
2 D. Chatterjee and S. Dasgupta, *J. Photochem. Photobiol., C*, 2005, **6**, 186–205.
3 F. Han, V. S. R. Kambala, M. Srinivasan, D. Rajarathnam and R. Naidu, *Appl. Catal., A*, 2009, **359**, 25–40.
4 E. Forgacs, T. Cserháti and G. Oros, *Environ. Int.*, 2004, **30**, 953–971.
5 X. L. Qu, J. Brame, Q. L. Li and P. J. J. Alvarez, *Acc. Chem. Res.*, 2013, **46**, 834–843.
6 N. Areerachakul, S. Vigneswaran, H. H. Ngo and J. Kandasamy, *Sep. Purif. Technol.*, 2007, **55**, 206–211.
7 H. K. Shon, S. Vigneswaran, H. H. Ngo and J. H. Kim, *Water Res.*, 2005, **39**, 2549–2558.
8 S. Kant, D. Pathania, P. Singh, P. Dhiman and A. Kumar, *Appl. Catal., B*, 2014, **147**, 340–352.
9 H. A. J. L. Mourão, V. R. de Mendonça, A. R. Malagutti and C. Ribeiro, *Quim. Nova*, 2009, **32**, 2181–2190.

Published on 22 January 2015. Downloaded by UNIVERSIDADE FEDERAL SAO CARLOS on 4/29/2019 6:13:09 PM.

10 F. F. de Brites-Nóbrega, A. N. B. Polo, A. M. Benedetti, M. M. D. Leão, V. Slusarski-Santana and N. R. C. Fernandes-Machado, *J. Hazard. Mater.*, 2013, **263**, 61–66.
11 L. Li, X. Liu, M. Gao, W. Hong, G. Z. Liu, L. Fan, B. Hu, Q. H. Xia, L. Liu, G. W. Song and Z. S. Xu, *J. Mater. Chem. A*, 2014, **2**, 1795–1801.
12 W. Li and S. Liu, *Adsorption*, 2012, **18**, 67–74.
13 M. Dawson, G. B. Soares and C. Ribeiro, *J. Nanosci. Nanotechnol.*, 2013, **7**, 5126–5133.
14 K. Li, Y. Tang, Y. Xu, Y. Wang, Y. Huo, H. Li and J. Jia, *Appl. Catal., B*, 2013, **140**, 179–188.
15 W. Kim, D. Pradhan, B. K. Minc and Y. Sohn, *Appl. Catal., B*, 2014, **147**, 711–725.
16 H. G. Wang, D. L. Ma, Y. Huang and X. Zhang, *Chem.–Eur. J.*, 2012, **18**, 8987–8993.
17 N. C. S. Vieira, W. Avansi, A. Figueiredo, C. Ribeiro, V. R. Mastelaro and F. E. G. Guimares, *Nanoscale Res. Lett.*, 2013, **7**, 310.
18 T. Gallasch, T. Stockhoff, D. Baither and G. Schmitz, *J. Power Sources*, 2011, **196**, 428–435.
19 V. Raju, J. Rains, C. Gates, W. Luo, X. Wang, W. F. Stickle, G. D. Stucky and X. Ji, *Nano Lett.*, 2014, **14**, 4119–4124.
20 B. Yan, L. Liao, Y. M. You, X. J. Xu, Z. Zheng, Z. X. Shen, J. Ma, L. M. Tong and T. Yu, *Adv. Mater.*, 2009, **21**, 2436–2440.
21 H. J. Liu, Y. F. Gao, J. D. Zhou, X. L. Liu, Z. Chen, C. X. Cao, H. J. Luo and M. Kanehira, *J. Solid State Chem.*, 2014, **214**, 79–85.
22 H. L. Fei, H. J. Zhou, J. G. Wang, P. C. Sun, D. T. Ding and T. H. Chen, *Solid State Sci.*, 2008, **10**, 1276–1284.
23 A. Kong, Y. J. Ding, P. Wang, H. Q. Zhang, F. Yang and Y. K. Shan, *J. Solid State Chem.*, 2011, **184**, 331–336.
24 V. R. de Mendonça and C. Ribeiro, *Appl. Catal., B*, 2011, **105**, 298–305.
25 X. Chen and S. S. Mao, *Chem. Rev.*, 2007, **107**, 2891–2959.
26 H. Li, R. Liu, Y. Liu, H. Huang, H. Yu, H. Ming, S. Lian, S. T. Lee and Z. Kang, *J. Mater. Chem.*, 2012, **22**, 17470–17475.
27 T. M. Milão, V. R. de Mendonça, V. D. Araújo, W. Avansi, C. Ribeiro, E. Longo and M. I. Bernardi, *Sci. Adv. Mater.*, 2012, **4**, 54–60.
28 J. Livage, *Materials*, 2010, **3**, 4175–4195.
29 Y. Zhang, C. Chen, W. Wu, F. Niu, X. Liu, Y. Zhong, Y. Cao and X. Liu, *Ceram. Int.*, 2013, **39**, 129–141.
30 W. Avansi, C. Ribeiro, E. R. Leite and V. R. Mastelaro, *Cryst. Growth Des.*, 2009, **9**, 3626–3631.
31 H. A. J. L. Mourao, W. Avansi, J. E. Oliveira, E. S. Firmiano and C. Ribeiro, *Sci. Adv. Mater.*, 2013, **5**, 71–85.
32 W. Avansi, C. Ribeiro, E. R. Leite and V. R. Mastelaro, *Mater. Chem. Phys.*, 2011, **127**, 56–61.
33 W. Avansi, R. Arenal, V. R. de Mendonca, C. Ribeiro and E. Longo, *CrystEngComm*, 2014, **16**, 5021–5027.
34 I. A. Castro, W. Avansi and C. Ribeiro, *CrystEngComm*, 2014, **16**, 1514–1524.
35 O. F. Lopes, E. C. Paris and C. Ribeiro, *Appl. Catal., B*, 2014, **144**, 800–808.
36 W. Avansi, C. Ribeiro, E. R. Leite and V. R. Mastelaro, *J. Cryst. Growth*, 2010, **312**, 3555–3559.
37 W. Avansi, L. J. Q. Maia, C. Ribeiro, E. R. Leite and V. R. Mastelaro, *J. Nanopart. Res.*, 2011, **13**, 4937–4946.
38 A. B. Murphy, *Sol. Energy Mater. Sol. Cells*, 2007, **91**, 1326–1337.
39 X. He, K. B. Male, P. N. Nesterenko, D. Brabazon, B. Paull and J. H. T. Luong, *ACS Appl. Mater. Interfaces*, 2013, **5**, 8796–8804.
40 G. C. Xi and J. H. Ye, *Chem. Commun.*, 2010, **46**, 1893–1895.
41 M. Shahid, L. Jingling, Z. Ali, I. Shakir, M. F. Warsi, R. Parveen and M. Nadeem, *Mater. Chem. Phys.*, 2013, **139**, 566–571.
42 K. Dai, J. L. Lv, L. H. Lu, Q. Liu, G. P. Zhu and D. P. Li, *Mater. Lett.*, 2014, **130**, 5–8.
43 S. C. Han, L. F. Hu, N. Gao, A. A. Al-Ghamdi and X. S. Fang, *Adv. Funct. Mater.*, 2014, **24**, 3725–3733.
44 X. Gao, F. Xiao, C. Yang, J. Wang and X. Su, *J. Mater. Chem. A*, 2013, **1**, 5831–5834.
45 J. Li, J. Feng and W. Yan, *Appl. Surf. Sci.*, 2013, **279**, 400–408.
46 V. R. de Mendonça, H. A. J. L. Mourão, A. R. Malagutti and C. Ribeiro, *Photochem. Photobiol.*, 2014, **90**, 66–72.
47 R. G. Harris, J. D. Wells and B. B. Johnson, *Colloids Surf., A*, 2001, **180**, 131–140.
48 G. Hahner, A. Marti, N. D. Spencer and W. R. Caseri, *J. Chem. Phys.*, 1996, **104**, 7749–7757.
49 Z. Y. Zhang and X. C. Xu, *Chem. Eng. J.*, 2014, **256**, 85–92.

 This journal is © The Royal Society of Chemistry 2015